International Journal of Latest Research in Engineering and Technology (IJLRET)
ISSN: 2454-5031
www.ijlret.com∥Volume 2 Issue 4∥April 2016 ∥PP 75-87

Prediction of airfoil lift coefficient in rain conditions using Artificial neural network

Zhenlong Wu[1,*], Yihua Cao[2]
[1] *National Laboratory of Aeronautics and Astronautics, Beihang University, Beijing 100191, China*
[2] *School of Aeronautic Science and Engineering, Beihang University, Beijing 100191, China*

A B S T R A C T: This paper presents the artificial neural network (ANN) model for predicting the lift coefficient aerodynamic performance of a NACA 64-210 airfoil in rain conditions. In order to determine the capability of the ANN technique on estimating the prediction value for lift coefficient, a wind-tunnel experiment is referred to in this study. in the experiment, 75 samples of data concerned with the airfoil lift coefficient in rain are selected. The MATLAB ANN toolbox is employed for the modeling purpose with some justifications. The Levenberg-Marquardt (trainlm), mean squared error (MSE), tangent sigmoid (tansig) for feedforward back-propagation networks is adopted as the training algorithm, performance and transfer functions, respectively. With three nodes in the input layer and one node in the output layer, eight network structures are chosen with different numbers of nodes in the hidden layer which are 3-1-1, 3-3-1, 3-6-1, 3-7-1, 3-1-1-1, 3-3-3-1, 3-6-6-1 and 3-7-7-1 structures. It is found that the 3-7-7-1 network structure gives the best prediction results of the lift coefficients of the airfoil in rain conditions. Finally, the effects of rain modeling parameters on the lift coefficients of the airfoil in rain conditions are discussed through a comparison between the experimental and the best 3-7-7-1 structure predicted results.

Keywords: ANN Airfoil Lift coefficient Rain

1 Introduction

Aerodynamic penalties of aircraft flight through heavy rain have been deemed to be a critical cause in many severe aviation accidents [1]. Heavy rain rate of 1800 mm/h can cause 30% decrease in lift and 20% increase in drag and also affect the stall angle, boundary-layer separation, flight safety and maneuverability. Meteorologists and aeronautical communities have been interested in rain associated with thunderstorms for decades.

Totally three approaches have been used to study aerodynamic performance of airfoils and wings in rain environment, i. e. flight test, wind-tunnel experiment and numerical simulation. Rhode firstly investigated rain effects on aircraft flight by wind tunnel test in 1941 [2]. Hermanspann [3], Adams [4] conducted flight tests to study rain effects on aircraft. Aerodynamic performance of airfoils [5-6] and wings [7] in rain was investigated via wind-tunnel experiments. As computational fluid dynamics (CFD) developed since the middle of 1990s, Valentine, et al. [8], Thompson, et al. [9], Ismail, et al. [10-11], Wu, et al. [12-13] simulated aerodynamic efficiency of airfoils and wings in rain by employing numerical simulation approach. Overall, the existing achievements show that rain can cause severe aerodynamic performance degradation to aircraft, namely decreases in lift and lift-to-drag ratio and increases in drag, thus threatens aircraft flight safety especially in a short-duration rain encounter.

Artificial neural networks emulate human functions such as learning from experience, generalizing and abstracting essential characteristics from input containing irrelevant data [14]. A detailed introduction of the development history of neural networks can be referred to in Ref. 15. Currently, neural networks have been performed by many governmental, industrial and academic research groups. Greenman, a researcher at NASA Ames research center, used neural networks to optimize the aerodynamic configuration of a two-dimensional high-lift airfoil [15]. Youssef and Juang used neural network technologies to provide a universal database for the storage and processing of flight test aerodynamic data [16]. In the field of effects of adverse weather conditions such as icing, neural networks have been applied to determine the potential relationships between ice shapes and aerodynamic performance [17].

With the very limited resources available for the problems involved in this study, i. e. airfoil lift coefficient in rain conditions, it is found that no study has yet focused on the issue of applying the ANN technique to predict airfoil lift coefficient in rain conditions. This issue could be assumed as the major contribution of this study to the area of aerospace engineering. In our study, the ANN technique is firstly employed to find the underlying relationships between some key modeling parameters of rain and aerodynamic lift coefficient in rain conditions. An understanding of the process of applying the ANN technique to develop the best model for the prediction of airfoil lift coefficient in rain conditions is outlined.

2 Modeling of lift coefficient in rain

In the field of aerospace engineering, lift coefficient C_L is as defined as follows:

$$C_L = \frac{L}{\frac{1}{2}\rho_a u_\infty{}^2 c} \tag{1}$$

where L is the lift, ρ_a and u_∞ are air density and free stream velocity, c is the airfoil chord length.

There are many factors determining the characteristics of rain which in turn affect the airfoil lift coefficient in rain conditions, such as raindrop diameter, rain intensity, terminal velocity of raindrop.

Marshall and Palmer developed the classic formula of the drop size distribution of thunderstorm rain based on massive experimental data [18], which can be expressed as follows.

$$N\left(D_p\right) = N_0 \exp\left(-ID_p\right) \quad \left(0 \le D_p \le D_{p_{\max}}\right) \tag{2}$$

where $N\left(D_p\right)$ ($\mathrm{m^{-3}mm^{-1}}$) is the number density of raindrops of diameter D_p (mm) per cubic meter of air, $D_{p_{\max}}$ is the maximum drop diameter. N_0 and I ($\mathrm{mm^{-1}}$) are parameters of $N\left(D_p\right)$ and have different values for different types of rain. For thunderstorm-type heavy rainfall as involved in our study, I varies with rainfall rate R as $I = 3.0 \times R^{-0.21}$, and N_0 has the constant value $N_0 = 1400\ \mathrm{m^{-3}mm^{-1}}$ [19] .

In experimental and numerical simulations, the rainfall rate (R) in millimeter per hour or the Liquid Water Content (LWC) in gram per cubic meter has been chosen to categorize different intensities of rainfall. A rainfall of rate of 100 mm/h or greater is often considered heavy rain. The correlation of the two factors depends on the type of rainfall. Multiplying the raindrop size distribution given by Eq. (2) by the raindrop mass and then integrating over the range of drop diameters will result in the relationship between (g/m^3) and (mm/h) for thunderstorm type rain [6]

$$LWC = 0.054R^{0.84} \tag{3}$$

It is assumed that raindrops have been with uniform velocity (i.e. without acceleration) before hitting the aircraft surface. So it is important to determine the terminal velocity (V_T) of raindrops. It was developed by Markowitz [20] as

$$V_T\left(m/s\right) = 9.58\left\{1 - \exp\left[-\left(\frac{D_p}{1.77}\right)^{1.147}\right]\right\} \tag{4}$$

3 Justification of ANN for C_L modeling

Although the application of the ANN model is widely utilized in various areas including aerospace engineering, there have been no clear rules that can serve as a basis to follow in producing a perfect model, the only way to obtain a successful model of ANN is by trial and error with consideration of some key factors. Due to this fact, this study considers the factors that can affect the effectiveness of the ANN model including the following fivefold:

- Network architecture.
- Network algorithm.
- Transfer function.
- Training function.
- Learning function.
- Performance function.
- Number of training data.
- Number of testing data.
- Normalization of input data.
- Anti-normalization of output data.

3.1 Network structure

An ANN structure or architecture usually consists of nodes and layers. Nodes are also called neurons. Layers usually include an input layer, one or more hidden layers and an output layer. An illustration of an ANN network with nodes and layers for our study is given in Fig. 1. It is worth mentioning that it is possible for an ANN architecture with no hidden layers. The network architecture has three nodes in the input layer which are dynamic pressure (q), liquid water content (LWC) and angle of attack (α), i nodes in the first hidden layer, j nodes in the second hidden layer, k nodes in the Nth hidden layer and one node, the output lift coefficient $\hat{C_L}$ in the output

layer. The example network in Fig. 1 can be defined as a 3-i-j-k-1 structure.

It is common sense that a network with more hidden layers and more nodes in each hidden layer can usually acquire a better prediction result but at the same time, more training and testing time and larger computer memories will be required. Too many nodes in hidden layers will lead to a waste of computer memory and computation time, while too few may not provide an ideal control effect [21]. The process of trial and error basis to obtain the best result is carried out by adjusting the number of hidden layers and the number of nodes in each hidden layer. Zhang, et al. [22] recommended that the number of nodes for the hidden layer are "n/2", "n", "2n" and "2n+1" where n denotes the number of nodes in the input layer. Since there are three input variables in this study, the number of nodes in each hidden layer according to Zhang, et al. are (3)/2=1.5≈1, 3, 2×3=6 and 2×3+1=7. Besides, with consideration of both computation expense and control effect, the trial and error process is limited with two hidden layers. Thus, eight network structures are applied in the current study, namely, 3-1-1, 3-3-1, 3-6-1, 3-7-1 for the network with a single hidden layer and 3-1-1-1, 3-3-3-1, 3-6-6-1, 3-7-7-1 for the network with two hidden layers, as illustrated in Fig. 2 and 3.

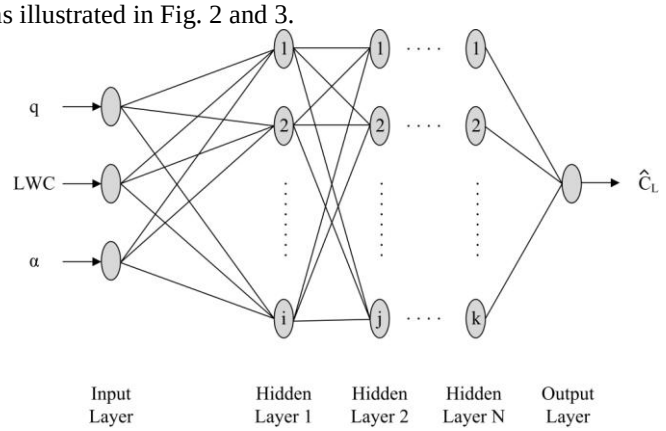

Fig. 1 Illustration of an ANN network architecture with nodes and layers in this study.

3.2 Amount of training and testing data

The amount of training and testing data for a network is a necessary consideration for all researchers. An increase in the amount of training and testing data will increase the chance of obtaining a more accurate model. In aerospace engineering, the actual experimental data are often used for network training. In this study, the wind-tunnel experimental data for the NACA 64-210 cruise configuration airfoil by Bezos, et al. [6] is adopted for the training of the eight networks. In Bezos's report, there are six groups with different experimental conditions for the NACA 64-210 cruise configuration airfoil, and the total number of sample size is 75.

3.3 Ratio of training and testing data

A desired network should be reached through both of the process of training and testing. For a set of sample data, usually a fraction of them is separated for training the network and the rest for testing. Basically, there is no general guideline to be followed to decide the ratio between the amounts of training and testing sample data. In other words, the ratio is often self-determined, as long as the amount of training samples is more than that of testing samples [23]. Percentwise, recommended ratios of training and testing samples given by Zhang, et al. [22] are 80%:20%, 85%:15% and 90%:10% with a total of 100% for the ratio of the available experimental samples. To fit with the experimental sample size of 75, the recommended amounts of training and testing samples are as follows:

(1) 75×80%+2=62 training samples,

(2) 75×20%-2=13 testing samples.

As is given in Table 1 for the normalized values of the ANN inputs and targets for training and testing, the total samples are separated into two groups as follows:

(1) samples No. 1 to No. 62 being selected for training,

(2) samples No. 63 to No. 75 being selected for testing.

3.4 Normalization of input data and anti-normalization of output data

Basically, when nonlinear transfer functions such as the logistic sigmoid function or hyperbolic tangent sigmoid function are used in the hidden layers, the input variables are in the interval of $(-\infty, +\infty)$ and the output variables in the interval of (-1, 1). In fact, the output can not necessarily be only in the interval of (-1, 1). When the absolute values of input variables are greater than a certain level, the output values will change slightly and the learning efficiency becomes very low, causing difficulty in convergence. Therefore, the input data are often limited to a certain range in order to avoid the aforementioned bad circumstances. In other words, the input sample data need to be normalized.

There are many ways to normalize the raw data of input, such as those given by Ezugwu, et al. [24] and Sanjay and Jyothi [25]. These approaches for normalization of data are somewhat complex for processing data. To simplify the data processing, a simple method is addressed here. With reference to the ranges of values of the input variables of q, LWC and α and the target variable T (experimental C_L), the normalization formulas are as follows:

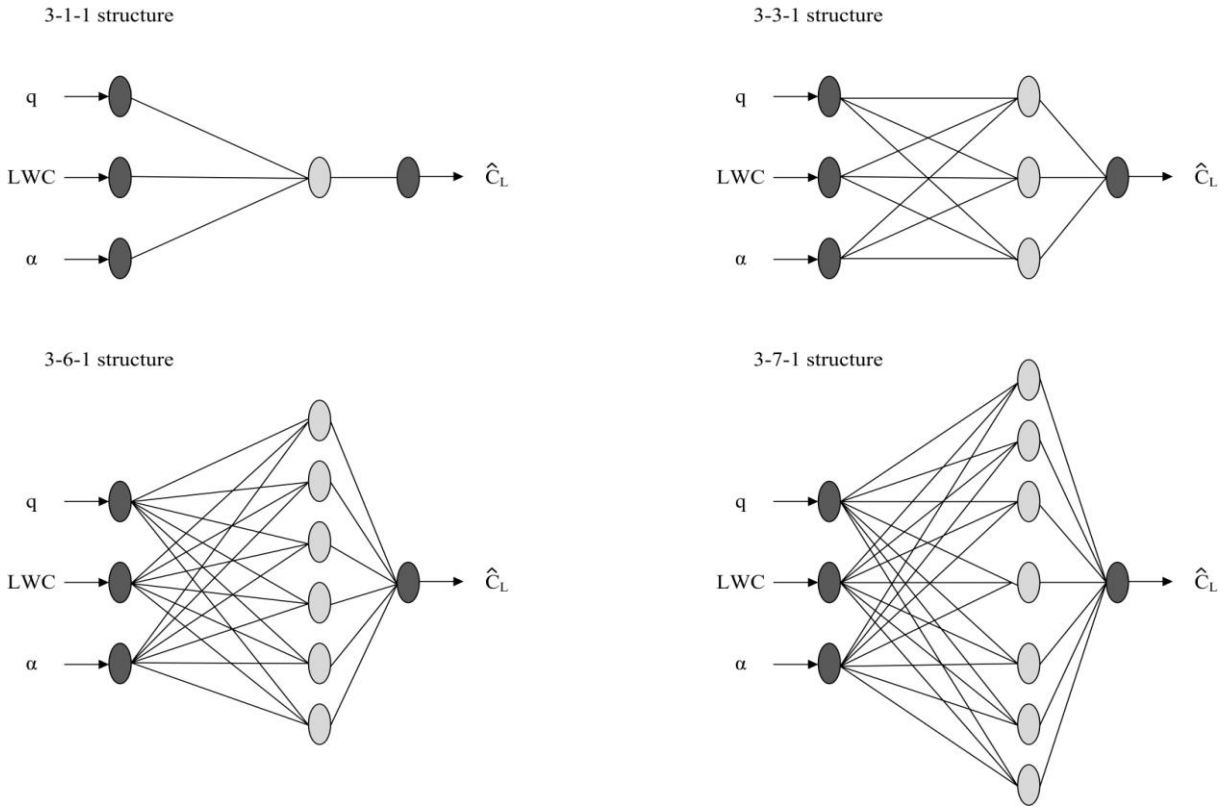

Fig. 2 Network structures with one hidden layer.

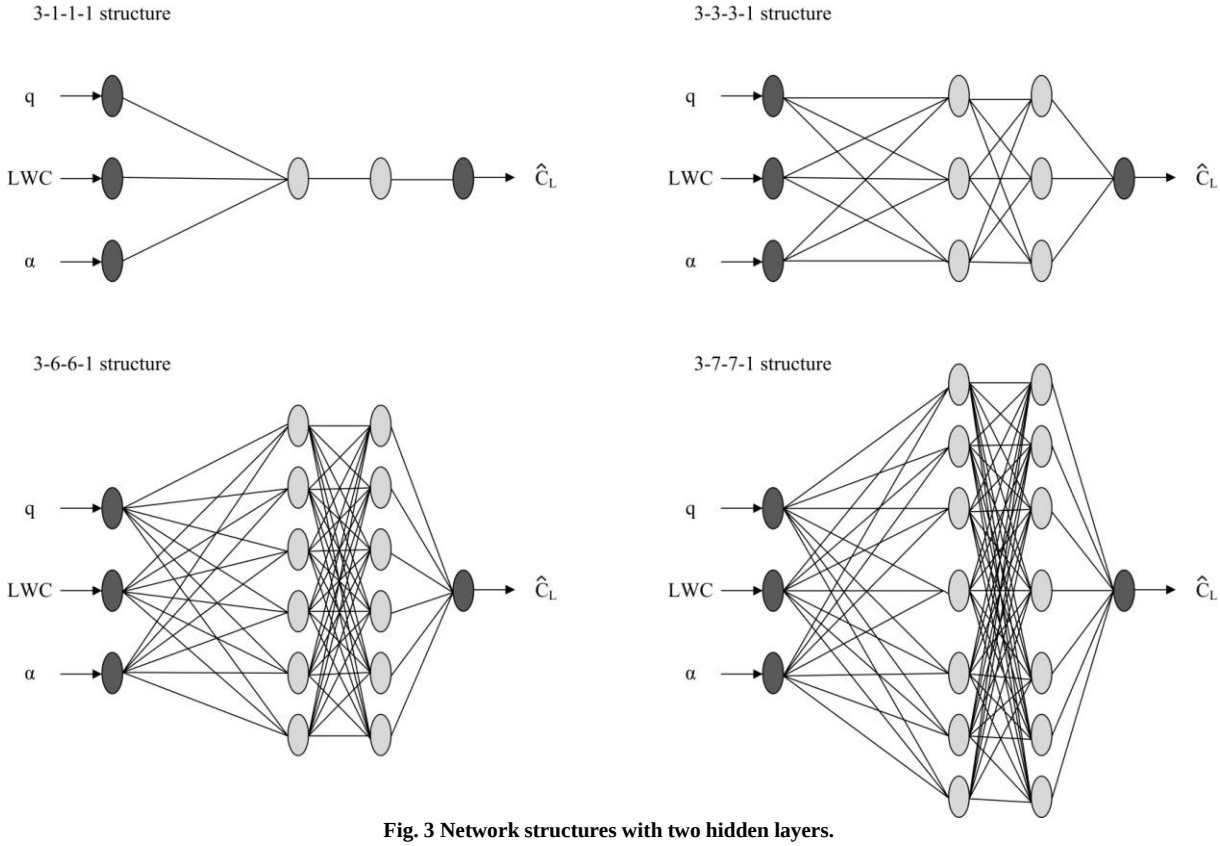

Fig. 3 Network structures with two hidden layers.

$$I_q = q/100 \quad (5)$$

$$I_{LWC} = LWC/100 \quad (6)$$

$$I_\alpha = \alpha/100 \quad (7)$$

The normalized values of the ANN inputs and targets are as listed in Table 1. When the optimal network is determined, the test samples will be set as the input to get the predicted results. For a direct comparison between the predicted results and the testing sample data (experimental), the predicted results $\hat{C}_L$ are usually anti-normalized from the network output O_{C_L}, which is given by

$$\hat{C}_L = 10O_{C_L} \quad (8)$$

Table 1. Values of the normalized ANN inputs and the non-normalized targets.

No.	I_q	I_{LWC}	I_α	T	No.	I_q	I_{LWC}	I_α	T
1	0.3	0	0	0.162	39	0.3	0.39	0.200 2	0.823
2	0.3	0	0.0203	0.336	40	0.5	0	0	0.161
3	0.3	0	0.0404	0.508	41	0.5	0	0.020 1	0.338
4	0.3	0	0.0609	0.680	42	0.5	0	0.040 0	0.511
5	0.3	0	0.0806	0.840	43	0.5	0	0.060 0	0.684
6	0.3	0	0.1002	1.003	44	0.5	0	0.080 8	0.858
7	0.3	0	0.1201	1.145	45	0.5	0	0.100 8	1.018
8	0.3	0	0.1300	1.207	46	0.5	0	0.120 8	1.160
9	0.3	0	0.1403	1.165	47	0.5	0	0.130 4	1.211
10	0.3	0	0.1509	1.121	48	0.5	0	0.140 5	1.156
11	0.3	0	0.1609	1.080	49	0.5	0	0.150 9	1.114
12	0.3	0	0.1802	1.076	50	0.5	0	0.160 4	1.102
13	0.3	0	0.2006	1.036	51	0.5	0	0.181 0	1.063
14	0.3	0.25	0	0.155	52	0.5	0	0.200 6	0.973
15	0.3	0.25	0.0207	0.326	53	0.5	0.19	0	0.160
16	0.3	0.25	0.0403	0.484	54	0.5	0.19	0.020 1	0.326
17	0.3	0.25	0.0608	0.658	55	0.5	0.19	0.040 2	0.492
18	0.3	0.25	0.0812	0.812	56	0.5	0.19	0.060 1	0.659
19	0.3	0.25	0.1009	0.952	57	0.5	0.19	0.080 3	0.818
20	0.3	0.25	0.1205	1.064	58	0.5	0.19	0.100 9	0.952
21	0.3	0.25	0.1300	1.101	59	0.5	0.19	0.120 4	1.046
22	0.3	0.25	0.1402	1.073	60	0.5	0.19	0.130 2	1.065
23	0.3	0.25	0.1505	1.020	61	0.5	0.19	0.139 9	1.031
24	0.3	0.25	0.1606	1.030	62	0.5	0.19	0.149 9	0.964
25	0.3	0.25	0.1800	0.949					

26	0.3	0.25	0.2006	0.894	63	0.5	0.3	0	0.153
27	0.3	0.39	0.0004	0.146	64	0.5	0.3	0.020 4	0.325
28	0.3	0.39	0.0205	0.315	65	0.5	0.3	0.040 3	0.485
29	0.3	0.39	0.0401	0.478	66	0.5	0.3	0.060 2	0.647
30	0.3	0.39	0.0607	0.639	67	0.5	0.3	0.080 2	0.799
31	0.3	0.39	0.0804	0.793	68	0.5	0.3	0.100 2	0.915
32	0.3	0.39	0.1005	0.928	69	0.5	0.3	0.120 7	1.010
33	0.3	0.39	0.1206	1.023	70	0.5	0.3	0.130 7	0.995
34	0.3	0.39	0.1306	1.061	71	0.5	0.3	0.139 9	0.965
35	0.3	0.39	0.1402	1.024	72	0.5	0.3	0.150 0	0.941
36	0.3	0.39	0.1500	0.942	73	0.5	0.3	0.160 3	0.920
37	0.3	0.39	0.1604	0.923	74	0.5	0.3	0.180 7	0.857
38	0.3	0.39	0.1804	0.868	75	0.5	0.3	0.201 7	0.805

3.5 Network algorithm

There are many network algorithms developed by researchers. In practical utilization of ANN network, back-propagation (BP) network algorithm or its varied forms are adopted in 80%-90% of ANN network models, thus the feedforward BP algorithm is adopted in the present study. But here the BP algorithm that we use is an improved BP algorithm named Levenberg-Marquardt (L-M algorithm) that will be depicted in the following subsection in detail. Generally, a feedforward network based on BP algorithm is an architecture consisting of one or more hidden layers located between the input and output layers. A typical feedforward network model with one hidden layer is as shown in Fig. 4. Every layer has both weights and biases for information transfer except the input layer. Now we proceed to derive the BP algorithm based on the feedforward network with one hidden layer in Fig. 4.

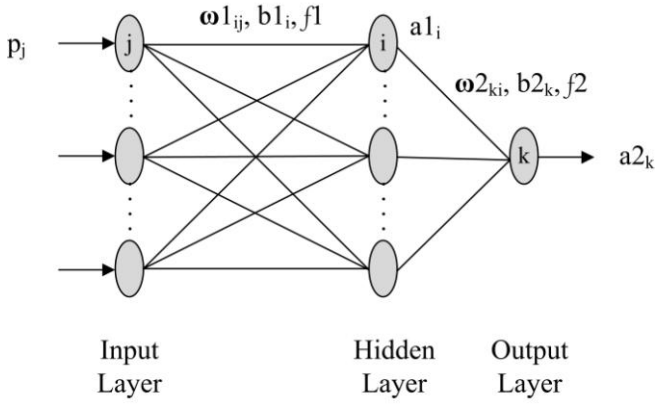

$k = 1, 2,\ldots, s2;\ I = 1, 2,\ldots, s1;\ j = 1, 2,\ldots, r$

Fig. 4 A typical feedforward network with a single hidden layer.

3.5.1 Feedforward of layer information

As shown in Fig. 4, assume that the input vector is P, and there are r input neurons, s1 neurons in the hidden layer and the transfer function from the input layer to the hidden layer is $f1$. Moreover, there are s2 neurons in the output layer, the corresponding transfer function is $f2$, the output vector is A and the target vector is T.

The net input to the output of node i in the hidden layer is expressed in Eq. (9),

$$a1_i = f1(\sum_{j=1}^{r} w1_{ij} p_j + b1_i) \quad (9)$$

Where p_j is the jth node of the input vector P, $w1_{ij}$ is the weight between the jth input neuron and the ith hidden neuron, $b1_i$ is the bias on the ith hidden node and $a1_i$ is the output of the ith hidden node.

The output of the kth neuron in the output layer is

$$a2_k = f2(\sum_{i=1}^{s1} w2_{ki} a1_i + b2_k) \quad (10)$$

where the parameters in the above equation can be easily deduced by referring to Eq. (9).

There are several transfer functions that could be used in MATLAB Neural Network Toolbox, such as hard limit transfer function (*hardlim*), linear transfer function (*purelin*), hyperbolic tangent sigmoid transfer function (*tansig*) and log-sigmoid transfer function (*logsig*). The *hardlim* transfer functions can only resolve simple classification problems, the *purelin* transfer function can well resolve linear problems, the last two sigmoid transfer functions are applied to nonlinear systems. In view of the strong nonlinearity in the current research system, only the sigmoid transfer functions can be utilized in our study. And the *tansig* transfer function is selected here due to its better computational accuracy in practice. The expression of the *tansig* transfer function is given in Eq. (11) as,

$$f = \frac{1 - e^{-2n}}{1 + e^{-2n}} \quad (11)$$

where n can be either the net of hidden nodes or the net of output nodes.

The error function that we use is called mean squared error (MSE) which is defined as follows,

$$MSE = \frac{1}{N} \sum_{k=1}^{N} (t_k - a2_k)^2 \quad (12)$$

where t_k is the target value of the kth output node.

3.5.2 Training algorithm

There are many training algorithms in the MATLAB Neural Network Toolbox, such as the standard Gradient-Descent algorithm, Variable Learning Rate algorithm (traingda, traingdx), Resilient Backpropagation algorithm (trainrp), Conjugate Gradient Algorithms (traincgf, traincgp, etc), Quasi-Newton Algorithms (trainbfg, trainoss), Levenberg-Marquardt algorithm (trainlm). The standard Gradient-Descent algorithm has some inherent shortcomings like long training time, potential slow adjustment of weights and biases and obtaining local minimal values of weights and biases. In addition, the Quasi-Newton Algorithms need to calculate the Hessian matrix (second derivatives) of the performance index at the current values of the weights and biases, which is complex and expensive to compute for feedforward neural networks. In our study, the Levenberg-Marquardt (L-M algorithm) is selected for network training. It has been widely used in engineering applications [26].

The L-M algorithm is a combination of the Gradient-Descent algorithm and the Quasi-Newton algorithms, which was designed to approach second-order training speed without having to compute the Hessian matrix. The L-M algorithm can be written as

$$X_{k+1} = X_k - [J^T J + \mu I]^{-1} J^T E \quad (13)$$

where X_k is a vector consisting of all the weights and biases in the network, J is the Jacobian matrix that contains first derivatives of the network errors with respect to the weights and biases [27], E is a vector of network errors, I is the unit matrix. μ is a scalar, when it equals zero, Eq. (13) becomes the Newton's method using the approximate Hessian matrix $H = J^T J$ and when it is large, Eq. (13) becomes the Gradient-Descent method with a small step size.

4 Determination of the best ANN model

The modeling results of $\hat{C}_L$ and the MSE values of $\hat{C}_L$ are generated by using the MATLAB Neural Network Toolbox with the learning rate of 0.01 and the initial values of all weights and biases of 0.1. With a total of 60 training samples, the modeling results of the $\hat{C}_L$ training phase are presented in Table 2. To determine the best network structure of the ANN prediction model, the two criteria considered in [23] are adopted in this work. The first criterion is the line pattern between the target values of lift coefficient T and the ANN output values $\hat{C}_L$ of the training phase. The second criterion is the consideration of the smallest value for the absolute average value of MSE of the testing phase to determine which network structure gives the best prediction for lift coefficient of the NACA 64-210 in rain.

In reference to the first criterion, the line patterns of the data between the ANN targets and outputs of the

training sample set is shown in Fig. 5 and Fig. 6 for the single-hidden-layer networks and two-hidden-layer networks, separately. The two graphs are generated by using the predicted values of $\hat{C}_L$ of all ANN structures in the training set listed in Table 2. It can be concluded that two network structures have the best similar form of line pattern between the targets lift coefficient T and the network predicted outputs $\hat{C}_L$, which are the 3-7-1 and 3-7-7-1 network structures. You may take it for granted that these networkstructures with more hidden nodes can always predict more accurate line patterns as is the same as the conclusion in the present work, however, Ref. 26 derived the conclusion that the 3-1-1-1 uncoated structure has the best similar form of line pattern of all the 8 uncoated structures and so do the 3-1-1 TiAIN coated and 3-1-1 SN_{TR} coated structures. Therefore, our work is not vain and has its value. In terms of the second criterion, The MSE values of the $\hat{C}_L$ testing

Table 2. Predicted values of lift coefficient $\hat{C}_L$ of all the ANN structures in the training phase.

No.	$\hat{C}_L$							
	3-1-1	3-3-1	3-6-1	3-7-1	3-1-1-1	3-3-3-1	3-6-6-1	3-7-7-1
1	0.202	0.207	0.158	0.166	0.179	0.165	0.166	0.160
2	0.326	0.338	0.340	0.340	0.338	0.337	0.336	0.337
3	0.494	0.505	0.510	0.504	0.524	0.506	0.505	0.512
4	0.689	0.691	0.674	0.672	0.681	0.682	0.676	0.680
5	0.870	0.864	0.835	0.845	0.833	0.846	0.842	0.834
6	1.016	1.011	1.011	1.018	1.006	0.998	1.009	1.010
7	1.114	1.115	1.155	1.145	1.143	1.151	1.148	1.152
8	1.142	1.144	1.181	1.171	1.175	1.175	1.175	1.172
9	1.157	1.155	1.170	1.166	1.178	1.164	1.168	1.161
10	1.159	1.144	1.133	1.135	1.158	1.136	1.137	1.135
11	1.148	1.113	1.094	1.097	1.127	1.106	1.104	1.107
12	1.100	1.075	1.052	1.068	1.070	1.058	1.061	1.062
13	1.017	1.060	1.054	1.034	1.025	1.040	1.034	1.032
14	0.150	0.143	0.158	0.149	0.138	0.157	0.154	0.159
15	0.300	0.303	0.331	0.327	0.325	0.323	0.327	0.322
16	0.479	0.480	0.491	0.485	0.494	0.484	0.489	0.488
17	0.673	0.669	0.651	0.646	0.643	0.656	0.652	0.656
18	0.847	0.842	0.808	0.813	0.814	0.815	0.814	0.806
19	0.970	0.973	0.962	0.969	0.981	0.953	0.967	0.959
20	1.040	1.052	1.073	1.074	1.074	1.081	1.077	1.079
21	1.055	1.066	1.086	1.089	1.080	1.092	1.089	1.091
22	1.059	1.062	1.071	1.076	1.064	1.072	1.071	1.074
23	1.049	1.036	1.035	1.039	1.033	1.038	1.035	1.039
24	1.029	0.990	0.996	0.995	1.000	1.002	0.998	1.001
25	0.966	0.935	0.936	0.952	0.951	0.942	0.947	0.942
26	0.871	0.882	0.895	0.903	0.894	0.907	0.907	0.906
27	0.128	0.118	0.145	0.147	0.125	0.149	0.149	0.150
28	0.286	0.286	0.315	0.321	0.312	0.313	0.318	0.310
29	0.468	0.468	0.481	0.478	0.472	0.474	0.477	0.478
30	0.663	0.660	0.645	0.636	0.624	0.647	0.638	0.648
31	0.821	0.823	0.790	0.788	0.794	0.793	0.788	0.786
32	0.936	0.950	0.932	0.935	0.956	0.922	0.935	0.925
33	0.994	1.019	1.027	1.028	1.025	1.036	1.032	1.032
34	1.002	1.027	1.033	1.035	1.018	1.037	1.036	1.038
35	0.999	1.016	1.014	1.015	0.995	1.011	1.012	1.014
36	0.985	0.986	0.979	0.974	0.963	0.974	0.974	0.974
37	0.960	0.933	0.937	0.922	0.930	0.932	0.932	0.928
38	0.887	0.879	0.868	0.868	0.885	0.861	0.868	0.858
39	0.790	0.822	0.820	0.817	0.814	0.819	0.816	0.822
40	0.193	0.182	0.161	0.155	0.173	0.158	0.157	0.166
41	0.326	0.325	0.340	0.348	0.345	0.333	0.338	0.335
42	0.499	0.499	0.510	0.510	0.526	0.508	0.513	0.510
43	0.690	0.687	0.675	0.670	0.676	0.687	0.684	0.686
44	0.876	0.874	0.850	0.856	0.840	0.862	0.861	0.855

45	1.015	1.024	1.028	1.039	1.014	1.027	1.032	1.021
46	1.101	1.125	1.160	1.163	1.131	1.170	1.164	1.162
47	1.122	1.149	1.178	1.181	1.149	1.185	1.184	1.184
48	1.131	1.154	1.166	1.167	1.141	1.169	1.169	1.173
49	1.128	1.136	1.135	1.130	1.115	1.137	1.130	1.138
50	1.114	1.099	1.102	1.092	1.085	1.102	1.092	1.100
51	1.055	1.064	1.042	1.062	1.030	1.030	1.032	1.028
52	0.969	0.963	0.978	0.973	0.984	0.983	0.994	0.990
53	0.157	0.155	0.158	0.149	0.147	0.164	0.161	0.161
54	0.306	0.309	0.332	0.343	0.332	0.331	0.334	0.322
55	0.490	0.488	0.501	0.501	0.503	0.498	0.499	0.496
56	0.679	0.671	0.659	0.648	0.649	0.660	0.652	0.664
57	0.849	0.841	0.811	0.807	0.818	0.806	0.804	0.813
58	0.975	0.975	0.963	0.965	0.989	0.947	0.955	0.954
59	1.040	1.046	1.053	1.052	1.070	1.055	1.051	1.053
60	1.053	1.054	1.053	1.053	1.071	1.053	1.055	1.057
61	1.054	1.040	1.024	1.024	1.052	1.024	1.027	1.025
62	1.043	1.003	0.975	0.973	1.022	0.981	0.978	0.969

Table 3. Differences between the targets T and predicted $\hat{C}_L$ of all the ANN structures in the testing phase.

No.	$T - \hat{C}_L$							
	3-1-1	3-3-1	3-6-1	3-7-1	3-1-1-1	3-3-3-1	3-6-6-1	3-7-7-1
63	0.019	0.021	0.017	0.018	0.029	0.004	0.016	0.020
64	-0.014	-0.009	-0.008	-0.008	-0.009	0.027	0.031	-0.001
65	-0.034	-0.029	-0.025	-0.025	-0.032	0.012	0.016	-0.019
66	-0.029	-0.023	-0.019	-0.019	-0.027	-0.002	0.001	-0.016
67	-0.004	0.001	0.004	0.004	-0.003	0.001	0.003	0.005
68	0.018	0.021	0.023	0.023	0.019	0.012	0.011	0.023
69	0.055	0.056	0.055	0.055	0.056	0.052	0.048	0.057
70	0.026	0.026	0.025	0.025	0.027	0.029	0.023	0.028
71	-0.008	-0.009	-0.010	-0.010	-0.007	0.001	-0.007	-0.006
72	-0.026	-0.028	-0.029	-0.029	-0.025	-0.011	-0.020	-0.024
73	-0.031	-0.033	-0.034	-0.034	-0.030	-0.011	-0.021	-0.028
74	-0.031	-0.031	-0.03	-0.03	-0.029	-0.010	-0.018	-0.025
75	0.024	0.031	0.038	0.037	0.025	0.024	0.024	0.034
MSE×10^{-4}	7.622	7.666	7.683	7.690	7.653	4.226	4.773	6.667

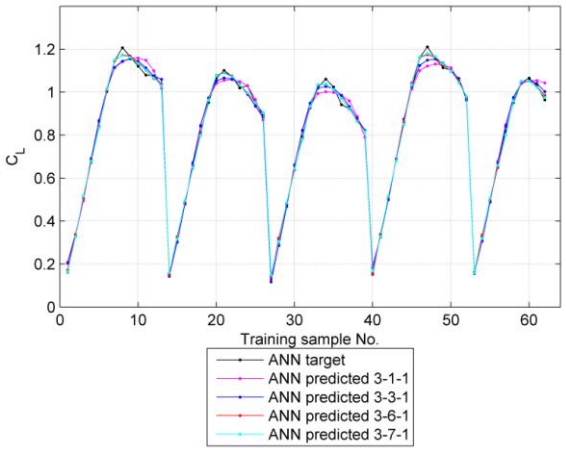

Fig. 5 Predicted lift coefficients of single-hidden-layer structures.

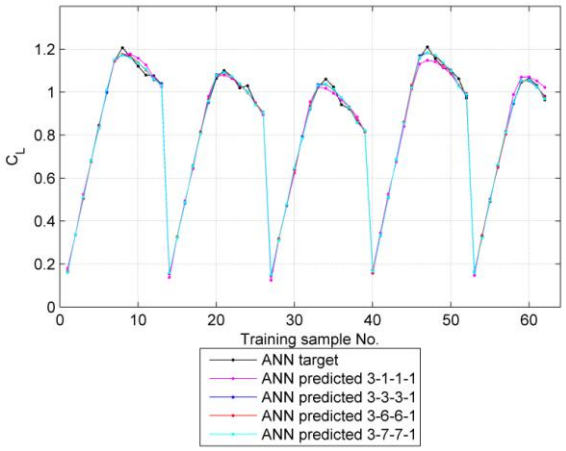

Fig. 6 Predicted lift coefficients of double-hidden-layer structures.

phase are presented in Table 3. It is clear that the 3-7-7-1 network structure has a lower MSE value of 6.667e-4 of the two best models. Thus, the 3-7-7-1 network structure is determined as the best model to predict lift coefficients of the NACA 64-210 airfoil in rain.

5 Analysis of the effects of rain modeling parameters on airfoil lift coefficients

The effects of LWC on the NACA 64-210 airfoil lift coefficients and the corresponding 3-7-7-1 ANN prediction results are as shown in Fig. 7 and Fig. 8 for q=30 and 50 psf, respectively. It can be seen from the two figures that relatively accurately fit the experimental data, especially at the relatively low angles of attack where the lift coefficient and angle of attack present a linear relationship. The maximum lift coefficient and the slope of the lift curve significantly decrease as LWC increases, which implies that the heavier the rain is, the more severe the aerodynamic lift penalty will be. In Fig. 7 where q=30 psf, the largest absolute decreases of lift coefficient occur at the largest angle of attack 20 degree, which are 0.142 and 0.213 for the experimental results at LWC 25 and 39 g/m^3, respectively, along with 0.126 and 0.210 for the ANN prediction results at LWC 25 and 39 g/m^3, respectively. And in Fig. 8 where q=50 psf, the largest absolute decreases of lift coefficient are 0.150 and 0.206 for the experimental results at LWC 19 and 30 g/m^3, respectively, along with 0.169 and 0.209 for the ANN prediction results at LWC 19 and 30 g/m^3, respectively.

The effects of dynamic pressure q on the NACA 64-210 airfoil lift coefficients and the corresponding 3-7-7-1 ANN prediction results are as shown in Fig. 9 and Fig. 10 for LWC=0 and 30 g/m^3, respectively. It can be seen that in the dry condition (no rain), the lift coefficients of the airfoil are nearly unaffected by dynamic pressure. However, in the rain condition of LWC 30 g/m^3, the lift characteristics at high angles of attack above 8 degree are dramatically changed by dynamic pressure. Moreover, it can be seen that at low angles of attack below 8 degree (including 8 degree), lift coefficients keep little changed at each angle of attack in both dynamic pressure conditions, while at angles of attack above 8 degree, lift coefficients decrease at each angle of attack as the dynamic pressure increases. This is a new and interesting phenomenon that has not been detected by predecessors in this field. It may be due to the physics that as the dynamic pressure or equally the free-stream velocity increases, trailing-edge flow separation at high angles of attack occurs or becomes more severe in the higher dynamic pressure condition, causing decreases in the lift coefficients. It can be concluded from this perspective that it is more advisable to conduct both experiment and numerical simulation of rain at low dynamic pressure conditions where lift characteristics are not greatly affected.

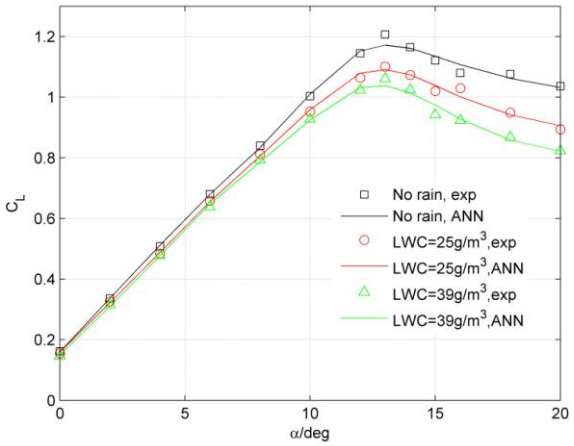

Fig. 7 Effects of LWC on the airfoil lift coefficients (q=30 psf).

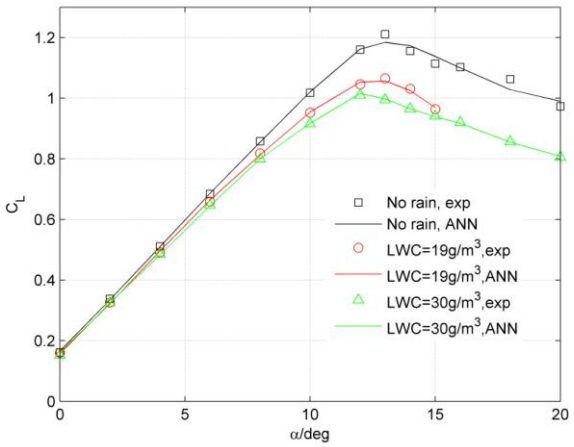

Fig. 8 Effects of LWC on the airfoil lift coefficients (q=50 psf).

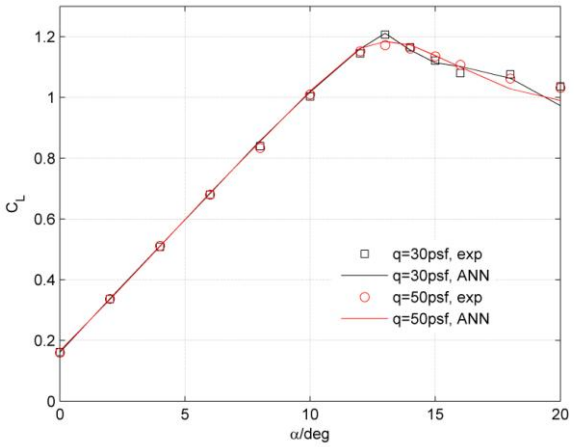

Fig. 9 Effects of q on the airfoil lift coefficients (LWC =0 g/m^3).

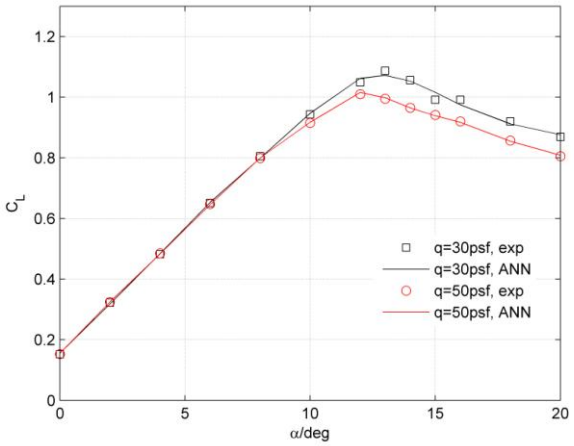

Fig. 10 Effects of q on the airfoil lift coefficients (LWC =30 g/m^3).

6 Conclusion

In this paper, a review of the current rain research situation and the ANN technique used in the field of aerospace engineering is presented. Considering that no study available has yet focused on the field of rain, it can be thought that this is the first attempt for the ANN technique to be used in the field of predicting lift coefficients of airfoil in rain conditions. Our object is to afford a new application area of the ANN technology as well as a new approach to study aerodynamic performance of airfoil in rain.

An important issue of concern in our work is the basic idea of ANN to be used for modeling lift coefficient in rain. In our viewpoint, the basic idea belongs to the understanding of the network structure of ANN. It is an important way of thinking for researchers to decide the number of layers and nodes in the hidden layers by trial and error to get a good prediction of the research object of interest. In our study, eight different network structures are selected for modeling based on literature recommendations, which are 3-1-1, 3-3-1, 3-6-1, 3-7-1, 3-1-1-1, 3-3-3-1, 3-6-6-1 and 3-7-7-1. Totally, seventy-five models are developed with the eight structures being applied to each model. It is found that the 3-7-7-1 structure gives the best prediction results of lift coefficient of the airfoil in rain conditions.

After having determined the best structure for predicting, a discussion of the effects of rain modeling parameters, LWC and dynamic pressure q, on the airfoil lift coefficient in rain are presented with data from both wind-tunnel experiment and the best ANN prediction structure. Some new phenomena are discovered and some new conclusions are drawn as to the lift performance of airfoil in rain conditions.

To conclude, this study is concerned about the artificial neural network technique for the model establishment to predict the values of lift coefficients of airfoil in rain conditions. It is called the modeling phase of the prediction of lift coefficients in rain which is important for providing the basic model for the foundation of the objective function. Considering that advantages of the ANN technique compared to wind-tunnel experiment are simplicity, speed, low cost, low risks, and capacity of learning, the ANN is a powerful tool in predicting the lift coefficients of airfoils in rain conditions.

Conflict of Interest

The authors declare that there is no conflict of interest regarding the publication of this manuscript.

References

[1]. Yihua Cao, Zhenlong Wu, Zhengyu Xu. Effects of rainfall on aircraft aerodynamics. Progress in Aerospace Sciences, 2014, 71: 85-127.
[2]. Rhode, R. V. Some effects of rainfall on flight of airplanes and on instrument indications, NASA TN-903, 1941.
[3]. Fred Hermanspann. Rain effects on natural laminar flow airfoils. AIAA paper 96-0899, 1996.
[4]. Adams, K. J. The Air Force Flight Test Center Artificial Icing and Rain Testing Capability. AIAA-83-2688, 1983.
[5]. Hansman, R. J. and Craig, A. P. Low Reynolds number tests of NACA 64-210, NACA 0012, and Wortman FX67-K170 airfoils in rain, Journal of Aircraft, 1987, 24, (8), pp 559-566.
[6]. Bezos, G. M., Dunham, R. E. and Gentry, G. L. and Melson, W. E. Wind tunnel aerodynamic characteristics of a transport-type airfoil in a simulated heavy rain environment, NASA TP-3184, 1992.
[7]. Thompson, B. E. and Jang, J. Aerodynamic performance of wings in rain, Journal of Aircraft, 1996, 33, (6), pp 1047-1053.

[8]. Valentine, J. R. and Decker, R. A. A Lagrangian-Eulerian scheme for flow around an airfoil in rain, Int. J. Multiphase Flow, 1995, 21, (4), pp 639-648.
[9]. Thompson, B. E. and Marrochello, M. R. Rivulet formation in surface-water flow on an airfoil in rain, AIAA Journal, 1999, 37, (1), pp 45-50.
[10]. Ismail, M., Yihua, C., Bakar, A., Zhenlong, W. Aerodynamic efficiency study of 2D airfoils and 3D rectangular wing in heavy rain via two-phase flow approach. Proceedings of the Institution of Mechanical Engineers, Part G: Journal of Aerospace Engineering, 2014, 228(7), pp 1141-1155.
[11]. Ismail, M., Yihua, C., Zhenlong, W., Amjad S. M. Numerical study of aerodynamic efficiency of a wing in simulated rain environment, 2014, Journal of Aircraft.
[12]. Zhenlong, W. and Yihua, C. Aerodynamic study of airfoil and wing in simulated rain environment via a two-way coupled Eulerian-Lagrangian approach, The Aeronautical Journal, June 2014, 118(1204) .
[13]. Zhenlong Wu and Yihua Cao. Numerical simulation of flow over an airfoil in heavy rain via a two-way coupled Eulerian-Lagrangian approach. International Journal of Multiphase Flow, 2015, 69: 81-92.
[14]. Grant, I. and Pan, X. An investigation of the performance of multi layer, neural networks applied to analysis of PIV images. Experiments in Fluids, 1995, 19, pp 159-166.
[15]. Greenman, R. M. Two-dimensional high-lift aerodynamic optimization using neural networks. NASA TM-1998-112233, 1998.
[16]. Youssef, H. M. and Juang, J. C. Estimation of aerodynamic coefficients using neural networks. AIAA-93-3639, 1993.
[17]. Pokhariyal, D., Bragg, M. B., Hutchison, T. and Merret, J. Aircraft flight dynamics with simulated ice accretion. AIAA-2001-0541, 2001
[18]. Marshall, J. S. and Palmer, W. K. The distribution of raindrops with size, Journal of Meteorology, 1948, 5, (4), pp 165-166.
[19]. Joss, J. and Waldvogel, A. Raindrop size distribution and sampling size errors, Journal of the Atmospheric Sciences, 1969, 26, (3), pp 566-569.
[20]. Markowitz, A. H. Raindrop size distribution expressions, Journal of Applied Meteorology, 1976, 15, (9), pp 1029-1031.
[21]. Al-Ahmari, A. M. A. Predictive machinability models for a selected hard material in turning operations. Journal of Material Processing Technology, 2007, 190, pp 305-311.
[22]. Zhang, G., Patuwo, B. E. and Hu, M. Y. Forecasting with artificial neural networks: The state of the art. International Journal of Forecasting, 1998, 14, pp 35-62.
[23]. Azlan M. Z., Habibollah H. and Safian, S. Prediction of surface roughness in the end milling machining using Artificial Neural Network. Expert Systems with Applications, 2010, 37(2010), pp 1755-1768.
[24]. Ezugwu, E. O., Fadare, D. A., Bonneya, J., Silva, R. B. D., & Sales, W. F. Modeling the correlation between cutting and process parameters in highspeed machining of Inconel 718 alloy using an artificial neural network. International Journal of Machine Tools and Manufacture, 2005, 45, pp 1375–1385.
[25]. Sanjay, C. and Jyothi, C. A study of surface roughness in drilling using mathematical analysis and neu-ral networks. International Journal of Advanced Manufacturing Technology, 2006, 29, pp 846–852.
[26]. Ilhan, A. and Mehmet, C. Modeling and prediction of surface roughness in turning operations using airtificial neural network and multiple regression method. Expert Systems with Applications, 2011, 38(2011), pp 5826-5832.
[27]. Hagan, M. T. and M. Menhaj. Training feedforward networks with the Marquardt algorithm. IEEE Transactions on Neural Networks, 1994, 5(6), pp 989–993.